Article

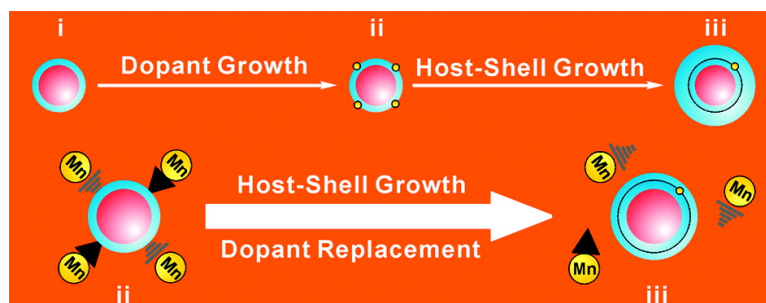# On Doping CdS/ZnS Core/Shell Nanocrystals with Mn

Yongan Yang, Ou Chen, Alexander Angerhofer, and Y. Charles Cao

More About This Article

Additional resources and features associated with this article are available within the HTML version:

- Supporting Information
- Access to high resolution figures
- Links to articles and content related to this article
- Copyright permission to reproduce figures and/or text from this article

View the Full Text HTML

On Doping CdS/ZnS Core/Shell Nanocrystals with Mn

Yongan Yang, Ou Chen, Alexander Angerhofer, and Y. Charles Cao*

Department of Chemistry, University of Florida, Gainesville, Florida 32611

Received July 22, 2008; E-mail: cao@chem.ufl.edu

Abstract: This paper presents a mechanistic study on the doping of CdS/ZnS core/shell semiconductor nanocrystals with Mn based on a three-step synthesis, which includes host-particle synthesis, Mn-dopant growth, and ZnS-shell growth. We used a combination of electron paramagnetic resonance spectroscopy (EPR) and inductively coupled plasma atomic emission spectroscopy (ICP) to monitor Mn-doping level and growth yield during doping synthesis at both the dopant-growth and ZnS-shell-growth steps. First, our kinetic study shows that Mn adsorption onto the nanocrystal surface includes the formation of weakly and strongly bound Mn. The formation of weakly bound Mn is associated with a chemical equilibrium between adsorbed Mn species on the nanocrystal surface and free Mn species in growth solution, while the formation of strongly bound Mn exhibits first-order kinetics with an activation-energy barrier of 211 ± 13 kJ/mol. Second, our results demonstrate that both weakly and strongly bound Mn can be removed from the surface of nanocrystals during ZnS-shell growth. The replacement of strongly bound Mn requires a higher temperature than that of weakly bound Mn. The yield of the replacement of strongly bound Mn is strongly dependent on the temperature of ZnS-shell growth. Third, our results show that the Mn-growth yield is not dependent on the size and crystal structure of nanocrystals. All together, these results suggest a mechanism in which nanocrystal doping is determined by the chemical kinetics of three activation-controlled processes: dopant adsorption, replacement, and ZnS-shell growth.

Introduction

The ability to precisely control impurity-doping in bulk semiconductors has enabled most modern semiconductor applications.[1,2] Doping with conventional impurities allows the control of the number of carriers (electrons and holes) in semiconductors, which has built the foundation for *p-n*-junction-based semiconductor devices, such as computer chips.[1] In addition, doping with magnetic impurities (e.g., Mn) has led to the development of dilute magnetic semiconductors (DMS).[3] These magnetic impurities can act as paramagnetic centers in the semiconductor lattice. Because of the *sp-d* exchange interaction between semiconductor host and magnetic impurities, bulk DMS crystals exhibit interesting magnetic and magneto-optical properties, which are critical for applications in spin-based electronics (i.e., spintronics).[4]

The importance of doping in bulk semiconductors has stimulated research efforts to develop synthetic methods to incorporate dopants into colloidal semiconductor nanocrystals.[5,6] However, *n*- and *p*-type doping of semiconductor nanocrystals

by conventional impurities has been unsuccessful through a colloidal synthesis, in part, because of the difficulties in introducing the impurities into colloidal nanocrystals.[5,7–9] Alternatively, most efforts have focused on doping semiconductor nanocrystals with magnetic impurities.[5] To date, a variety of semiconductor nanocrystals have been doped with Mn, as well as other magnetic impurities such as Co, Ni, Eu, and Tb.[6,10–35]

(1) Sapoval, B.; Hermann, C. *Physics of semiconductors*; Springer-Verlag: New York, 1993.

(2) Yu, P. Y.; Cardona, M. *Fundamentals of semiconductors*; Springer: New York, 1995.

(3) Aggarwal, R. L.; Furdyna, J. K.; von Molnar, S. *Diluted Magnetic (Semimagnetic) Semiconductors*; MRS Symposia Proceedings: Pittsburgh, PA, 1987; Vol. 89.

(4) Wolf, S. A.; Awschalom, D. D.; Buhrman, R. A.; Daughton, J. M.; von Molnar, S.; Roukes, M. L.; Chtchelkanova, A. Y.; Treger, D. M. *Science* **2001**, *294*, 1488–1495.

(5) Shim, M.; Wang, C.; Norris, D. J.; Guyot-Sionnest, P. *MRS Bulletin* **2001**, 1005–1009.

(6) Erwin, S. C.; Zu, L.; Haftel, M. I.; Efros, A. L.; Kennedy, T. A.; Norris, D. J. *Nature* **2005**, *436*, 91–94.

(7) Shim, M.; Guyot-Sionnest, P. *Nature* **2000**, *407*, 981–983.

(8) Wang, C. J.; Shim, M.; Guyot-Sionnest, P. *Science* **2001**, *291*, 2390–2392.

(9) Yu, D.; Wang, C. J.; Guyot-Sionnest, P. *Science* **2003**, *300*, 1277–1280.

(10) Bhargava, R. N.; Gallagher, D.; Hong, X.; Nurmikko, A. *Phys. Rev. Lett.* **1994**, *72*, 416–419.

(11) Sooklal, K.; Cullum, B. S.; Angel, M.; Murphy, C. J. *J. Phys. Chem.* **1996**, *100*, 4551–4555.

(12) Ji, T.; Jian, W. B.; Fang, J. *J. Am. Chem. Soc.* **2003**, *125*, 8448–8449.

(13) Mikulec, F. V.; Kuno, M.; Bennati, M.; Hall, D. A.; Griffin, R. G.; Bawendi, M. G. *J. Am. Chem. Soc.* **2000**, *122*, 2532–2540.

(14) Magana, D.; Perera, S. C.; Harter, A. G.; Dalal, N. S.; Strouse, G. F. *J. Am. Chem. Soc.* **2006**, *128*, 2931–2939.

(15) Stowell, C. A.; Wiacek, R. J.; Saunders, A. E.; Korgel, B. A. *Nano. Lett.* **2003**, *3*, 1441–1447.

(16) Somaskandan, K.; Tsoi, G. M.; Wenger, L. E.; Brock, S. L. *Chem. Mater.* **2005**, *17*, 1190–1198.

(17) Suyver, J. F.; Wuister, S. F.; Kelly, J. J.; Meijerink, A. *Phys. Chem. Chem. Phys.* **2000**, *2*, 5445–5448.

(18) Counio, G.; Gacoin, T.; Boilot, J. P. *J. Phys. Chem. B* **1998**, *102*, 5257–5260.

(19) Hoffman, D. M.; Meyer, B. K.; Ekimov, A. I.; Merkulov, I. A.; Efros, A. L.; Rosen, M.; Couino, G.; Gacoin, T.; Boilot, J. P. *Solid State Commun.* **2000**, *114*, 547–550.

(20) Norris, D. J.; Yao, N.; Charnock, F. T.; Kennedy, T. A. *Nano. Lett.* **2001**, *1*, 3–7.

(21) Zu, L. J.; Norris, D. J.; Kennedy, T. A.; Erwin, S. C.; Efros, A. L. *Nano Lett.* **2006**, *6*, 334–340.

In general, two types of synthetic methods have been developed to produce doped nanocrystals.[5,6] The first method is based on aqueous-phase coprecipitation, or inverse micelle templates.[33,34] This method often leads to nanoparticle products with low crystallinity and broad size distributions.[5] The second method is organic-phase growth, which can produce monodisperse and highly crystalline colloidal nanocrystals.[6,13,20,26] In many cases, the impurity atoms exist only at the surface of the nanocrystals—not inside the core—therefore minimizing the impurity's effects on the nanocrystal's properties.[5,13] Gamelin et al. have introduced a method of using isocrystalline shell growth to incorporate surface impurities inside the cores.[36] Peng et al. have reported that impurity-doping can be decoupled from the nanocrystal nucleation and growth stages.[28] Based on this progress, we have developed a three-step synthesis to achieve radial-position-controlled doping of semiconductor nanocrystals.[26] We have shown the first example in which optical properties of Mn-doped CdS/ZnS nanocrystals strongly depend on Mn radial positions inside the host core/shell nanocrystals. In addition, we have synthesized Mn-doped CdS/ZnS nanocrystals with a room-temperature Mn-emission quantum yield (QY) of 56%.[26] Please note that Peng et al. have recently reported that Mn-doped ZnSe nanocrystals made by their improved method exhibit Mn-emission QY of ∼50%).[30,37] Nanocrystals with such a high-emission QY are very important to applications such as nanocrystal-based biomedical sensing.[38–41] More recently, Ithurria et al. discovered that Mn dopants can be used as a radial pressure gauge to measure local strain within CdS/ZnS core/shell nanocrystals.[42]

Despite such exciting progress, the mechanisms of nanocrystal-doping synthesis have not yet been fully understood. There is still controversy about a fundamental question: what controls dopant incorporation in a colloidal nanocrystal-doping synthesis?

Two important models have been proposed to explain the Mn-doping of semiconductor nanocrystals.[6,43–46] Chelikowsky et al. suggested a doping-growth model in which self-purification is an intrinsic property of defects in semiconductor nanocrystals.[43–45] They proposed that doping is determined by the formation energy of Mn impurities inside semiconductor nanocrystals. From a DFT (density functional theory) calculation, Chelikowsky et al. show that the formation energy of Mn impurities increases as the size of the nanocrystal decreases. In this model, the size of nanocrystals is important for incorporating dopants into the nanocrystal lattice. This model is based on an assumption that Mn-dopant incorporation is under a thermodynamic equilibrium. However, such a thermodynamic equilibrium is normally not established in an organic-phase synthesis performed at 200–350 °C, because the diffusion of Mn is negligible at these growth temperatures.[6,46]

Norris et al. proposed a Mn-doping model called "trapped dopant", in which dopant incorporation is governed by dopant growth kinetics.[6,46] On the basis of a DFT calculation of Mn-surface binding energy, they argue that the crystal structure and shape of nanocrystals are two major factors that affect Mn-doping.[6] The theoretical results show that Mn is more easily incorporated into zinc-blende nanocrystals than into those with wurtzite or rocksalt structures. In addition, they suggest that surfactant binding energy is also an important factor for dopant incorporation.[6] Most importantly, the Norris model provides the first quantitative prediction on dopant-growth yield (or doping efficiency) for a colloidal synthesis.[6] For ZnSe nanocrystals exhibiting the equilibrium shape, Mn-growth yield is predicted to range between 0 and 30%. This prediction can explain the observation that Mn-growth yield is often ∼10% in a one-pot doping synthesis.[6,20,21] This prediction also seems consistent with our recent results that Mn-growth yield of ∼30% was achieved in a three-step synthesis.[26] However, the Norris model cannot explain the results from Gamelin et al., that a Mn-growth yield of ∼40% was achieved in Mn-doping of wurtzite ZnO nanocrystals.[35] In addition, this model cannot explain the doping synthesis using the active polychalcogenide precursors that incorporate Mn in cluster form as a prebonded Se–Mn complex.[6,12,13]

Furthermore, both theoretical doping models are based on the experimental results obtained from a conventional one-pot doping synthesis by Norris et al.[6] In such a synthesis, Mn-dopant precursors and host-growth precursors are mixed together for producing doped nanocrystals. The dopant-adsorption process and host-lattice growth occur concurrently in the synthesis. Thus it is extremely difficult to obtain quantitative kinetic data on the dopant adsorption process, which is important for establishing a general doping model.

To overcome this difficulty, we have used the synthesis of Mn-doped CdS/ZnS core/shell nanocrystals as a model system, and carried out a mechanistic study of dopant incorporation on the basis of a three-step doping synthesis (Scheme 1). This doping synthesis separates a conventional one-pot nanocrystal-doping synthesis into three independent steps: (1) synthesis of "host particles", (2) dopant growth (Mn-dopants are adsorbed on the surface of host particles in this step), and (3) host-shell

(22) Bryan, J. D.; Gamelin, D. R. *Prog. Inorg. Chem.* **2005**, *54*, 47–126.
(23) Chengelis, D. A.; Yingling, A. M.; Badger, P. D.; Shade, C. M.; Petoud, S. *J. Am. Chem. Soc.* **2005**, *127*, 16752–16753.
(24) Beaulac, R.; Archer, P. I.; Liu, X.; Lee, S.; Salley, G. M.; Dobrowolska, M.; Furdyna, J. K.; Gamelin, D. R. *Nano Lett.* **2008**, *8*, 1197–1201.
(25) Olano, E. M.; Grant, C. D.; Norman, T. J.; Castner, E. W.; Zhang, J. Z. *J. Nanosci. Nanotech.* **2005**, *5*, 1492–1497.
(26) Yang, Y.; Chen, O.; Angerhofer, A.; Cao, Y. C. *J. Am. Chem. Soc.* **2006**, *128*, 12428–12429.
(27) Norman, T. J.; Magana, D.; Wilson, T.; Burns, C.; Zhang, J. Z.; Cao, D.; Bridges, F. *J. Phys. Chem. B* **2003**, *107*, 6309–6317.
(28) Pradhan, N.; Goorskey, D.; Thessing, J.; Peng, X. *J. Am. Chem. Soc.* **2005**, *127*, 17586–17587.
(29) Bol, A. A.; van Beek, R.; Meijerink, A. *Chem. Mater.* **2002**, *14*, 1121–1126.
(30) Pradhan, N.; Peng, X. *J. Am. Chem. Soc.* **2007**, *129*, 3339–3347.
(31) Hanif, K. M.; Meulenberg, R. W.; Strouse, G. F. *J. Am. Chem. Soc.* **2002**, *124*, 11495–11502.
(32) Raola, O. E.; Strouse, G. F. *Nano. Lett.* **2002**, *2*, 1443–1447.
(33) Yang, H. S.; Holloway, P. H.; Ratna, B. B. *J. Appl. Phys.* **2003**, *93*, 586–592.
(34) Yang, H. S.; Santra, S.; Holloway, P. H. *J. Nanosci. Nanotech.* **2005**, *5*, 1364–1375.
(35) Norberg, N. S.; Kittilstved, K. R.; Amonette, J. E.; Kukkadapu, R. K.; Schwartz, D. A.; Gamelin, D. R. *J. Am. Chem. Soc.* **2004**, *126*, 9387–9398.
(36) Radovanovic, P. V.; Gamelin, D. R. *J. Am. Chem. Soc.* **2001**, *123*, 12207–12214.
(37) Pradhan, N.; Battaglia, D. M.; Liu, Y.; Peng, X. *Nano. Lett.* **2007**, *7*, 312–317.
(38) Alivisatos, A. P. *Nat. Biotechnol.* **2004**, *22*, 47–52.
(39) Han, M.; Gao, X.; Su, J. Z.; Nie, S. *Nat. Biotechnol.* **2001**, *19*, 631–635.
(40) Rosi, N. L.; Mirkin, C. A. *Chem. Rev.* **2005**, *105*, 1547–1562.
(41) Jin, R. C.; Wu, G. S.; Li, Z.; Mirkin, C. A.; Schatz, G. C. *J. Am. Chem. Soc.* **2003**, *125*, 1643–1654.
(42) Ithurria, S.; Guyot-Sionnest, P.; Mahler, B.; Dubertret, B. *Phys. Rev. Lett.* **2007**, *99*, 265501.

(43) Dalpian, G. M.; Chelikowsky, J. R. *Phys. Rev. Lett.* **2006**, *96*, 226802.
(44) Dalpian, G. M.; Chelikowsky, J. R. *Phys. Rev. Lett.* **2008**, *100*, 179703.
(45) Du, M. H.; Erwin, S. C.; Efros, A. L.; Norris, D. J. *Phys. Rev. Lett.* **2008**, *100*, 179702.
(46) Norris, D. J.; Efros, A. L.; Erwin, S. C. *Science* **2008**, *319*, 1776–1779.

Scheme 1. Three-Step Synthesis for Synthesizing Mn-Doped CdS/ZnS Core/Shell Nanocrystals[a]
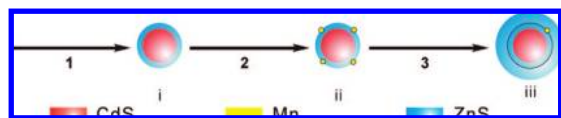
[a] (1) synthesis of host particles, (2) Mn-dopant growth, and (3) host-shell growth; (i) host particles, (ii) particles with surface-bound Mn, and (iii) final particles.

growth (i.e., ZnS-shell growth in this work). On the basis of this synthesis, we have monitored the nanocrystal doping levels (the concentration of dopants on a nanocrystal) and dopant-growth yield in both the dopant-growth and ZnS-shell-growth steps, separately. We have studied the dopant-growth yield as a function of the following synthesis variables: the size, crystal structure of host particles, the composition of doping precursors, as well as the reaction temperatures for the dopant-growth and ZnS-shell-growth steps.

Our results show that the adsorption of Mn dopants onto the nanocrystal surface starts from the formation of weakly bound Mn, and then is followed by a chemical reaction to form strongly bound Mn. We have identified that the formation of strongly bound Mn needs to overcome an activation-energy barrier of 211 ± 13 kJ/mol. Moreover, our results demonstrate that both the weakly and strongly bound Mn can be replaced during ZnS-shell growth, and the yield of Mn-replacement reaction is strongly dependent on the growth temperature. In addition, we find that Mn-dopant incorporation is not affected by the size or crystal structure of host particles in our experiments. All together, these results are consistent with a mechanism in which nanocrystal doping is controlled by the kinetics of three activation-controlled processes: Mn adsorption and replacement, and ZnS-shell growth (a process of embedding Mn atoms into the host lattice). We have shown that the reaction kinetics can be controlled by the composition of doping precursors, and the temperatures at the dopant-growth and ZnS-shell-growth steps. Based on this new insight, we have demonstrated the ability to control the dopant-growth yield up to 80%. We hope these results will prove useful in the design of new doping syntheses for producing high-quality, doping-based nanomaterials for applications such as biomedical diagnosis, photocatalysts, solar cells, light-emitting devices, spintronic devices, etc.[5,24,37−41,46]

Experimental Section

A. Chemicals. Sulfur powder (99.999%), 1-octadecene (ODE, tech. 90%), oleylamine (OAm, tech. 70%), 1-octadecylamine (ODA, 97%), Trioctylphosphine oxide (TOPO, 99%) and tributylphosphine (TBP, 90%), were purchased from Aldrich. Manganese acetate tetrahydrate (99%) and all the solvents were purchased from Fisher Scientific Company. Bis(2,4,4-trimethylpentyl) phosphinic acid (BTMPPA) (90%,, tech.), and nitric acid (≥69.5%, TraceSELECT) were purchased from Fluka. Cadmium acetate hydrate (99.999%), cadmium oxide (99.998%), zinc stearate (count as ZnO% ≈ 14%) and selenium (200 mesh, 99.999%) were purchased from Alfa Aesar. Quinine sulfate (99+%) was purchased from Acros. The chemicals were used as received without further purification. Cadmium myristate and manganese diethyldithiocarbonate ($Mn(S_2CNEt_2)_2$) were self-made according to the literature methods.[26,47]

B. Stock Solutions. (1) Mn(OAc)$_2$ Solution. OAm (4 mL) was added into a 25-mL flask and heated at 120 °C for 10 min under a vacuum of 20 mTorr. After the oleylamine solvent was cooled to

room temperature, $Mn(OAc)_2 \cdot 4H_2O$ (4.9 mg, 0.02 mmole) was quickly added into the flask. The mixture was degassed at room temperature and at 120 °C for 10 min for each step. After a clear solution was obtained, the solution was cooled to room temperature and ready for use. Note that the Mn-precursor solution should be freshly made before the synthesis.

(2) Mn(S$_2$CNEt$_2$)$_2$ Solution.[26] An OAm solution of $Mn(OAc)_2$ (2 mL, 10 mM) was prepared according to the protocol above, and then an oleylamine solution of NaS_2CNEt_2 (2 mL, 22 mM) was made in pretreated oleylamine at 60 °C under Ar flow. Then the NaS_2CNEt_2 solution was added into the $Mn(OAc)_2$ solution at 60 °C with stirring under Ar flow. After 10 min, a slightly yellow solution of $Mn(S_2CNEt_2)_2$ was obtained and was used directly for dopant growth. Note that the Mn-precursor solution should be freshly made before the synthesis.

(3) Sulfur Solution. Sulfur powder (12.8 mg, 0.4 mmol) was added into a flask with ODE (10 mL). After degassing at room temperature for 10 min, the solution was heated to 130 °C under Ar flow. The temperature was maintained for 5 min, and then the resulting sulfur solution was cooled to room temperature for use. Caution should be taken to avoid heating the solution to a higher temperature.

(4) Zinc-Stearate Solution. Zinc-stearate powder (0.4 mmol) was added into a flask with ODE (10 mL). After degassing at room-temperature for 10 min, the mixture was heated to 200 °C to dissolve zinc stearate. The solution was cooled to room temperature and a slurry formed. The slurry was directly used for ZnS shell growth.

C. Sample Preparation. (1) Synthesis of CdS/ZnS Core/ Shell Nanocrystals. Zinc-blende CdS/ZnS core/shell nanocrystals were prepared according to the literature method.[26] First, zinc-blende CdS nanocrystals were prepared using a noninjection synthesis.[48] In a typical synthesis, cadmium myristate (1.0 mmol) and sulfur (0.5 mmol) were added into a flask with 50 g of ODE. The resulting mixture was degassed at room temperature, and then was heated to 240 °C under Ar flow. The nanocrystal growth was monitored using UV−vis spectroscopy. When the nanocrystals reached 3.1 nm in diameter, the synthesis solution was cooled to room temperature. CdS nanocrystals were precipitated using acetone, and redispersed in toluene. The typical samples have a size distribution of 7% and the first exciton absorption peak at 400 nm. Second, ZnS shells were grown onto the resulting CdS nanocrystals at 220 °C in a mixture solution of ODE and OAm with a volume ratio of 3:1. The ZnS shells were grown monolayer by monolayer, by alternate injections of zinc-stearate solution (40 mM) in ODE and sulfur in ODE (40 mM). Growth time was 10 min after each injection. When the desired shell thickness was achieved, the growth solution was cooled to room temperature. The resulting Cds/ZnS core/shell nanocrystals were precipitated by using acetone, and redispersed in hexane. In addition, we also synthesized wurtzite CdS/ZnS core/shell nanocrystals according to the method developed by Bawendi et al.[49] In this paper, these zinc-blende and wurtzite CdS/ZnS nanocrystals were used as host particles to study the doping mechanism in the following dopant-growth and ZnS-shell-growth steps.

(2) Dopant Growth. In a typical experiment, a hexane solution of host particles (2 mL, 50.4 nmol) was added into a mixture solution of ODE and OAm (8.0 mL, ODE/OAm: 3:1), and then hexane was removed under vacuum. Under Ar flow, the nanocrystal solution was heated to a growth temperature (i.e., 180−280 °C), and doping precursors (0.2−2.4 μmol, $Mn(OAc)_2$ and sulfur at a molar ratio of 1:1, or $Mn(S_2CNEt_2)_2$) were introduced into the solution by dropwise addition. The additional amount is equivalent to 4−48 Mn atoms per nanocrystal. After the addition, dopant growth was allowed for 20 min, and was stopped by cooling the

(47) Coucouvanis, D. *Prog. Inorg. Chem.* **1970**, *11*, 233–371.

(48) Cao, Y. C.; Wang, J. *J. Am. Chem. Soc.* **2004**, *126*, 14336–14337.

(49) Steckel, J. S.; Zimmer, J. P.; Coe-Sullivan, S.; Stott, N. E.; Bulovic, V.; Bawendi, M. G. *Angew. Chem., Int. Ed.* **2004**, *43*, 2154–2158.

reaction solution to room temperature. Then the resulting nanocrystals were purified via precipitation by adding acetone, and redispersed in toluene as a high-concentration solution for further use. For electron paramagnetic resonance (EPR) or inductively coupled plasma atomic emission spectroscopy (ICP), the samples were further purified by three precipitation-redispersion cycles using methanol and toluene.

(3) ZnS-Shell Growth. In a typical experiment, a toluene solution of the resulting particles after dopant growth (1 mL, 25.2 nmol) was added into a mixture solution of ODE and OAm (4.0 mL, ODE/OAm: 3:1), and then toluene was removed under vacuum. Under Ar flow, the nanocrystal solution was heated to a target growth temperature (220−280 °C). The ZnS shell was grown monolayer by monolayer, by alternate injections of zinc-stearate solution (40 mM) in ODE and sulfur in ODE (40 mM). Growth time was 10 min after each injection. After the desired shell thickness was achieved, an additional zinc-stearate solution (0.12 mmol) in ODE was added to the reaction system. After 5 min the synthesis was stopped by cooling the reaction solution to room temperature, and the nanocrystals were purified via precipitation by adding acetone. The resulting nanocrystals were further purified by three precipitation-redispersion cycles using methanol and toluene. For EPR or ICP measurements, the samples were further purified twice by a pyridine-exchange treatment according to a literature method.[6,13,21] After the treatment, the resulting particles were dispersed in pyridine. Then the pyridine-capped particles were further exchanged with TOPO and dodecylamine (1:1), and redispersed in toluene. Please note that we have found that the order of the alternate precursor injections can affect the Mn-doping levels of final CdS/ZnS core/shell particles (vide infra). In this paper, the ZnS growth was conducted by the injection of Zn precursors first, unless mentioned otherwise.

D. Kinetic Study of Mn Adsorption. (1) Formation of Weakly Bound Mn. In a typical experiment, 4.1-nm CdS/ZnS core/shell nanocrystals with 3.1-nm CdS cores (150 nmol) were loaded into a mixture solution of ODE and OAm (12.0 mL, ODE/OAm: 3:1). Under Ar flow, the nanocrystal solution was heated to the growth temperatures (180, 220, or 240 °C), and doping precursors (Mn(OAc)$_2$ and sulfur at a molar ratio of 1:1, 7.2 μmol, an amount equivalent to 48 atoms per nanocrystal) were added. After the addition, aliquots (1.5 mL) were taken periodically during dopant growth. The nanocrystals in the aliquots were purified by three precipitation/redispersion cycles for EPR and ICP measurements.

(2) Formation of Strongly Bound Mn. In a typical experiment, 4.1-nm CdS/ZnS core/shell nanocrystals with 3.1-nm cores (500 nmol) were loaded into a mixture solution of ODE and oleylamine (40 mL, ODE/oleylamine: 3:1). Under Ar flow, the nanocrystal solution was heated to the growth temperatures (250, 260, 270, or 280 °C), and doping precursors (Mn(OAc)$_2$ and sulfur at a molar ratio of 1:1, 24 μmol, an amount equivalent to 48 atoms per nanocrystal) were added. After the addition, aliquots (∼5 mL) were taken periodically during dopant growth. The nanocrystals in the aliquots were purified by three precipitation/redispersion cycles.

To remove the weakly bound Mn species from the purified particles, ZnS-shell growth was conducted at 220 °C with zinc stearate and sulfur as precursors. The thickness of the ZnS shell is approximately 1.5 monolayers. After the ZnS-shell growth, the resulting particles were purified according to the procedures described above. The Mn-doping levels of these particles obtained by ICP were used to determine the amount of strongly bound Mn formed in the dopant-growth step.

E. Characterizations. (1) Absorption Spectra. UV−vis absorption spectra were measured using a Shimadzu UV1701. Nanocrystals were dissolved in toluene for the measurement.

(2) Measurement of Photoluminescence. Photoluminescence (PL) and photoluminescence excitation (PLE) experiments were performed on a fluorometer (Fluorolog-3, Horiba Jobin Yvon, Irvine, CA). Room-temperature fluorescence quantum yields of Mn-

doped nanocrystals were determined by using literature methods.[50] Briefly, quinine sulfate in 0.5 M of H$_2$SO$_4$ solution was used as a reference standard, of which the concentration was adjusted to have an absorbance between 0.05 and 0.1 at its peak position of 348 nm. A toluene solution of Mn-doped CdS/ZnS nanocrystals was also adjusted to a concentration with equal absorbance intensity to that of quinine sulfate.

(3) Electron Paramagnetic Resonance (EPR). The EPR measurements were performed in CW mode on an X-band Bruker Elexsys 580 spectrometer (9.5 GHz) using an Oxford ESR900 cryostat (all the experiments were performed at a temperature of 6 K). The samples were treated by pyridine exchange twice according to literature methods.[6,13,21] The purified nanocrystals were dissolved in a toluene solution with 10% polystyrene to form a glass upon freezing.

(4) Inductively Coupled Plasma Atomic Emission Spectroscopy (ICP). The ICP measurements were performed on a Vista RL CCD Simultaneous ICP-AES (Varian, Inc.). The purified nanocrystal samples were digested with nitric acid (69.5%). The digestion was performed at about 100 °C until the solution became colorless. The digestion solutions were further diluted with a nitric-acid solution to obtain a final nitric-acid concentration of about 1−2%. The concentrations of Mn, Cd, and Zn in solutions were determined by data from ICP measurements as compared with the corresponding working curve.

The Mn-doping level (Mn-DL) is defined as

$$\text{Mn-DL} = \frac{[\text{Mn}]}{[\text{Cd}] + [\text{Zn}] + [\text{Mn}]}$$

In addition, Mn-doping level is also described as the number of Mn atoms per nanocrystal. The number was calculated using the size of the CdS core determined by TEM and the ratio of [Mn]/[Cd] determined by ICP.

The Mn-growth yield (Mn-GY) is defined as

$$\text{Mn-GY} = \frac{\text{Mn}_{\text{ICP}}}{\text{Mn}_{\text{Added}}}$$

where Mn$_{\text{ICP}}$ is the total amount (mol) of Mn in nanocrystal samples, which is determined by ICP measurements, and Mn$_{\text{Added}}$ is the amount (mol) of Mn added as doping precursors at the dopant-growth step.

The Mn-replacement yield (Mn-RY) is defined as

$$\text{Mn-RY} = 1 - \frac{\text{GY}_2}{\text{GY}_1}$$

where GY$_1$ and GY$_2$ are measured after the dopant-growth and ZnS-shell-growth steps, respectively.

(5) Transmission Electron Microscopy (TEM). A toluene solution of the purified nanocrystals was dropped onto carbon-coated copper grids and dried in air and kept overnight in a vacuum desiccator. The TEM images were acquired on a JEOL transition electron microscope (200 kV).

(6) X-ray Diffraction (XRD). A concentrated toluene solution of the purified nanocrystals was dropped onto a low-scattering quartz sample-holder and dried in air and kept overnight in a vacuum desiccator. The XRD measurements were performed on a Philips XRD 3720 spectrometer.

Results and Discussion

Quantitative Determination of Doping Level and Mn-Growth Yield. We used a combination of EPR and ICP to determine Mn-doping level and growth yield for the mechanistic study of Mn-doping synthesis. EPR was used to determine the location

(50) Demas, J. N.; Crosby, G. A. *J. Phys. Chem.* **1971**, *75*, 991−1024.
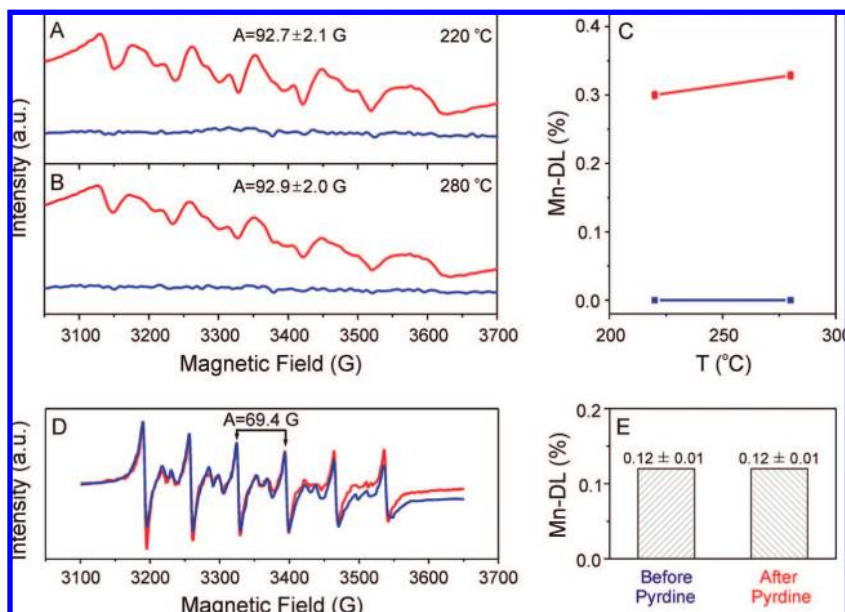
Figure 1. EPR spectrum of 4.1-nm CdS/ZnS core/shell nanocrystals with surface-bound Mn (in red) and that of the control (in blue): synthesized at 220 °C (A), and 280 °C (B). (C) ICP data for the Mn-doping level (Mn-DL) of the two nanocrystal samples (in red) and their corresponding controls (in blue): the Mn-DL is equivalent to an average of 2.5 Mn per particle for the sample made at 220 °C, and 2.8 Mn for the sample made at 280 °C. (D) EPR spectrum of 4.1-nm CdS/ZnS core/shell nanocrystals with Mn incorporated inside ZnS shell before (in blue) and after (in red) pyridine-exchange treatment. (E) ICP data for the corresponding nanocrystal samples: the DL is equivalent to an average of 4 Mn atoms per particle.

of Mn atoms, and ICP was used to quantitatively measure the Mn-doping level of nanocrystals and Mn-growth yield in the dopant-growth and ZnS-shell-growth steps.

In the dopant-growth step, Mn atoms are adsorbed onto the surface of 4.1-nm CdS/ZnS core/shell nanocrystals. To determine whether Mn atoms are indeed on the surface of nanocrystals, we carried out four sets of experiments. The first two sets of experiments were conducted at 220 and 280 °C. In these experiments, dopant precursor (Mn-acetate and S at a molar ratio of 1:1 with an amount of 4 Mn atoms per nanocrystal) was added into growth solutions (4 mL, ODE and OAm at a ratio of 3:1) with CdS/ZnS nanocrystals (25.2 nmol). After growth for 20 min, the growth solutions were cooled to room temperature. The nanocrystals were isolated from growth solutions, and further purified by three precipitation-redispersion cycles. Resulting nanocrystals were redispersed in toluene.

X-band EPR shows that typical samples from these two sets of experiments exhibit a broad six-line spectrum (red lines in Figure 1A-B), which arises due to the hyperfine interaction with the [55]Mn nuclear spin ($I = 5/2$).[6,51] EPR spectra have a similar hyperfine coupling constant (A) of about 92.8 G (red lines in Figure 1A−B). Such a large hyperfine coupling constant is close to that of Mn in octahedral sites.[13,52,53] This result suggests that Mn atoms are bound on the surface of nanocrystals. However, these EPR data cannot rule out the possibility that Mn atoms are in molecular complexes dispersed in the nanocrystal toluene solutions.

To examine this possibility, we carried out two sets of corresponding control experiments, in which only Mn precursors were added into the reaction solutions at 220 and 280 °C without host particles. After heating for 20 min at the corresponding temperatures, the solutions were cooled to room temperature,

and 4.1-nm CdS/ZnS nanocrystals were added. Then nanocrystals were isolated from the solutions, and further purified by three precipitation-redispersion cycles as before. The resulting particles were redispersed in toluene and used as control samples. Both EPR and ICP measurements show no measurable Mn signals from these control samples (blue lines in Figure 1A−C). These results unambiguously demonstrate that the observed Mn signals do not arise from any Mn molecular complexes dispersed in the nanocrystal toluene solutions, but rather come from the Mn atoms bound to the surface of the CdS/ZnS nanocrystals. More importantly, these results also suggest that the incorporation of Mn atoms onto the nanocrystal surface was achieved through dopant growth at the reaction temperatures, but not due to the subsequent purification treatment at room temperature. Therefore, the data from quantitative ICP measurements should represent the actual Mn-doping levels of the resulting nanocrystals. Accordingly, the Mn-growth yield for each reaction was calculated as the ratio of $[Mn]_{ICP}$ to $[Mn]_{Added}$.

In the ZnS-shell-growth step, surface-bound Mn atoms can be incorporated into the lattice of the ZnS shell in the resulting particles (Scheme 1). EPR measurements show that typical samples exhibit a narrow six-line spectrum with a hyperfine coupling constant of about 69.7 G (red line in Figure 1D). Such a hyperfine coupling constant indicates that the Mn dopants are at cubic ZnS lattice sites,[51,53,54] and thus the dopants are indeed located inside the core/shell nanocrystals. Interestingly, the sample before pyridine treatment shows a nearly identical EPR spectrum (blue line in Figure 1D) to that of the sample after pyridine treatment (red line in Figure 1D). In addition, ICP measurements show that these two samples have a nearly identical doping level (Figure 1E). These results indicate that these Mn-doped nanocrystals have a very "clean" surface, and the amount of surface-bound Mn is not detectable by either EPR

(51) Kennedy, T. A.; Glaser, E. R.; Klein, P. B.; Bhargava, R. N. *Phys. Rev. B* **1995**, *52*, R14356.
(52) Igarashi, T.; Isobe, T. *Phys. Rev. B* **1997**, *56*, 6444–6445.
(53) Griscom, D. L.; Griscom, R. R. *J. Chem. Phys.* **1967**, *47*, 2711–2722.

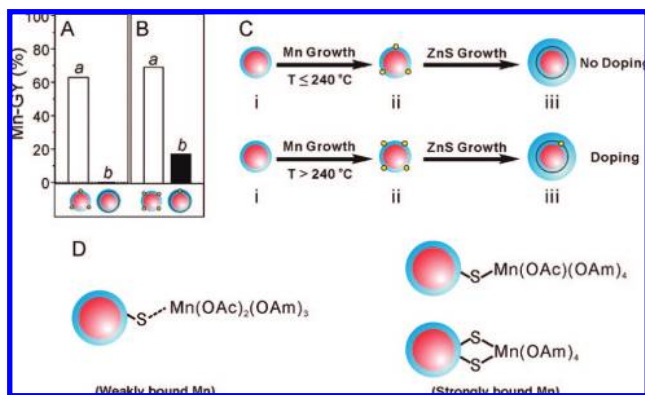(54) Koh, A. K.; Miller, D. J. *Solid State Commun.* **1986**, *60*, 217–222.

Figure 2. Mn-growth yield (Mn-GY) measured by ICP after the dopant-growth and ZnS-shell-growth steps: (A) $T = 220\ °C$ and (B) $T = 280\ °C$; Column *a*: taken after dopant-growth step, and column *b*: taken after the growth of 0.5-nm ZnS shell. (C) Schematic for Mn adsorption and replacement. (i) Host particle, (ii) particle with Mn at surface, (iii) final particle. (D) Schematic for the proposed structures of the weakly and strongly bound Mn species on the surface of CdS/ZnS core/shell nanocrystals.

or ICP. In other words, the Mn species that are not incorporated into the lattice of CdS/ZnS core/shell nanocrystals should exist in reaction solutions, and they can be easily removed by the purification procedure using three precipitation/redispersion cycles. In our experiments, however, the pyridine-exchange treatments were still performed before the ICP measurements to rule out potential errors in determining the Mn-doping levels of the resulting nanocrystals. On the basis of the doping levels determined by ICP, we calculated the net Mn-growth yield after ZnS-shell growth as described above.

Weakly Bound Mn and Strongly Bound Mn. Here we used Mn-growth yield and the doping level of nanocrystals as the two key parameters to study the Mn-doping-growth mechanism in the doping synthesis. We found that the dopant growth can lead to both weakly and strongly bound Mn adsorbed onto the surface of CdS/ZnS core/shell nanocrystals. Moreover, we found that ZnS-shell growth is a sufficient procedure to distinguish the weakly bound Mn from strongly bound ones, because ZnS-shell growth can easily remove the weakly bound Mn, but not the strongly bound ones (Figure 2).

In the mechanistic study herein, we chose 4.1-nm CdS/ZnS core/shell nanocrystals as host particles and a mixture of ODE and OAm (3:1) as growth solutions, while keeping the particle concentration (6.3 μM) and dopant-precursor concentration (0.3 mM) unchanged in the doping experiments. With manganese acetate and sulfur as precursors, doping growth leads to a Mn-growth yield of about 63% in the experiment at a growth temperature of 220 °C, and a yield of 69% at 280 °C (Figure 2A-a, 2B-a).

After ZnS-shell growth, however, nearly all the surface-bound Mn atoms were removed from the host particles prepared in the experiment with the dopant growth at 220 °C, which resulted in a net Mn-growth yield of nearly zero (Figure 2A-b). This result indicates that these Mn dopants are just weakly adsorbed on the surface of host particles at this low-temperature growth condition (called weakly bound Mn).

In contrast, for the experiment with Mn-dopant growth at 280 °C, the ZnS-shell growth only removes about three-fourths of Mn atoms from host particles, and results in a net Mn-growth yield of about 17% for the doping experiment (Figure 2B-b). Therefore, at least one-fourth of Mn atoms are strongly adsorbed

on the surface of host particles in this high-temperature dopant-growth condition (called strongly bound Mn).

Interestingly, before ZnS-shell growth, the core/shell nanocrystals with strongly bound Mn do not exhibit a distinguishable EPR spectrum as compared to those without strongly bound Mn (red lines in Figure 1A and B). These EPR data show that the formation of strongly bound Mn does not substantially change the Mn coordinating environment on the surface of CdS/ZnS core/shell nanocrystals. These EPR data further indicate that both weakly bound and strongly bound Mn exist as molecular complexes with a six-coordination environment around Mn (II) centers (e.g., acetate and/or OAm as chelating ligands).[51,53] Altogether, these results suggest that the weakly bound Mn complexes likely serve as Lewis-acid ligands which bind onto the Lewis-base sites (i.e., sulfur sites) on the surface of CdS/ZnS core/shell nanocrystals via weak coordination bonds, whereas the strongly bound Mn complexes are attached onto the nanocrystal surface through one or more strong Mn−S bonds (Figure 2D).

In addition, our results show that the Mn-doping level is not detectable for the CdS/ZnS core/shell nanocrystals prepared in the experiments with the dopant-growth and ZnS-shell-growth temperature at 240 °C, but the doping level is detectable for the nanocrystals in the experiments conducted at higher temperatures (Figure 2C). This temperature-dependent phenomenon strongly suggests that the adsorption of Mn dopants is determined by the kinetics of chemical reactions between Mn precursors and nanocrystal surface atoms.

Kinetics of Mn-dopant adsorption. The kinetics of Mn adsorption were studied by monitoring the Mn-growth yield as a function of time during dopant growth at different temperatures. For the formation of the weakly bound Mn, we studied the growth kinetics at three temperatures (180, 220 and 240 °C) because only weakly bound Mn can be formed at these conditions. Aliquots were taken periodically during dopant growth, and the resulting particles were purified by three precipitation/redispersion cycles for ICP measurements. ICP data show that Mn-growth yields reach about 63% at 1 min after the addition of dopant precursors (Mn-acetate and S at a molar ratio of 1:1 at an amount of 48 Mn per nanocrystal) (Figure 3A). The Mn-growth yields remain nearly constant during further growth at the three growth temperatures (Figure 3A). These ICP data indicate that Mn adsorption reaches a steady state after only 1 min. This result is consistent with the conclusion that weakly bound Mn complexes are a type of "ligand" on the nanocrystal surface: the formation of weakly bound Mn includes "ligand" adsorption and desorption processes, and the two processes can rapidly reach a chemical equilibrium in the growth solutions at these reaction temperatures (Scheme 2).[55]

To further confirm the establishment of equilibrium between the adsorption/desorption processes, we injected a sulfur precursor solution (the amount of S is 12 times larger than that of Mn in the growth solution) into a dopant-growth solution at 220 °C. Sulfur can introduce more Lewis-base sites on the surface of CdS/ZnS core/shell nanocrystals, and thus the nanocrystals should adsorb more free Mn complexes from the growth

(55) Ji, X.; Copenhaver, X.; Sichmeller, C. *J. Am. Chem. Soc.* **2008**, *130*, 5726–5735.
(56) Atkin, P. W. *Physical Chemistry*, 6th ed.; Oxford University Press: Oxford, 1998.
(57) Connors, K. A. *Chemical kinetics: the study of reaction rate in solution*; VCH Publishers, Inc.: New York, 1990.
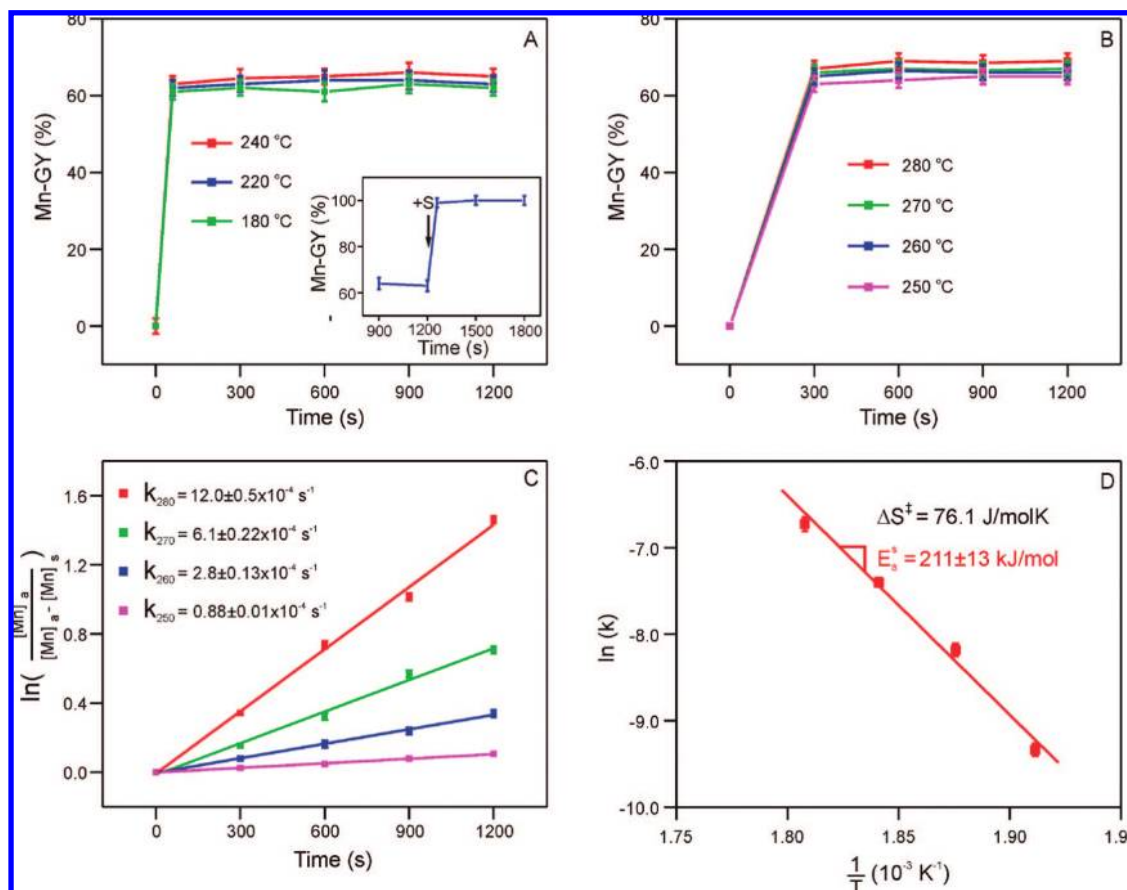
Figure 3. Kinetic study of Mn adsorption. The formation of weakly bound Mn: (A) Mn-growth yield (Mn-GY) as a function of time at three different temperatures (180, 220, and 240 °C, indicated by green, blue, and red lines, respectively). (Inset) The Mn-GY changes due to the injection of a sulfur precursor solution at 1200 s in the experiment at 220 °C. The formation of strongly bound Mn: (B) Mn-GY before ZnS growth as a function of time at four different temperatures (250, 260, 270, and 280 °C, indicated by purple, blue, green, and red lines, respectively). (C) A plot of ln $\{[Mn]_a/([Mn]_a - [Mn]_s)\}$ versus time (s). $[Mn]_a$ is the concentration of total adsorbed Mn on the surface of nanocrystals determined by ICP before ZnS growth, and $[Mn]_s$ is the concentration of strongly bound Mn on the surface of nanocrystals determined by ICP after ZnS growth. The first-order rate constants (k_T) are extracted from the plots. (D) Arrhenius plot of ln(k) verses 1/T. Activation energy (E_a^s) and the entropy of activation ($\Delta S^{\ddagger}$) are extracted from the plot.

solution. Indeed, ICP measurements show that the Mn-growth yield rapidly reaches nearly 100% after the injection, and the growth yield remains unchanged afterward (insert, Figure 3A). This result further confirms that there is an equilibrium between Mn adsorption/desorption processes. Although our current experimental data are not sufficient to determine the rate constant of adsorption (k_1) and desorption (k_{-1}) processes (Scheme 2), this issue does not substantially affect the kinetic study on the formation of strongly bound Mn.

For the formation of the strongly bound Mn, we studied the growth kinetics at four temperatures (250, 260, 270 and 280 °C). Aliquots were taken periodically during dopant growth, and the resulting particles were purified for ICP measurements. Because both weakly bound and strongly bound Mn form under these conditions, the Mn-doping level obtained from the direct ICP measurements of the resulting particles includes the contributions from these two types of Mn. Surprisingly, ICP measurements show that Mn-growth yields also remain nearly constant during dopant growth in these experiments (Figure 3B). The growth yields do not exhibit strong temperature dependence, but the yields are just slightly higher than those yields obtained from the experiments at lower temperatures (Figure 3A–B).

These results suggest that there is also an equilibrium between the adsorption and desorption of Mn complexes in growth solutions, and the formation of strongly bound Mn does not substantially affect the equilibrium. This suggestion is consistent with the fact that the formation of strongly bound Mn does not increase the number of Lewis-base sites on the surface of nanocrystals. Thus the overall equilibrium achieved in these experiments is between the concentration of the total adsorbed Mn on nanocrystals and the concentration of free Mn complexes in the growth solution at these temperatures.

To quantitatively analyze the concentration of strongly bound Mn on the resulting particles in these four experiments (i.e., at 250, 260, 270 and 280 °C), we conducted a ZnS-shell growth at 220 °C to remove the weakly bound Mn species from the surface of CdS/ZnS core/shell nanocrystals. After the ZnS-shell growth, the core/shell nanocrystals were purified by three precipitation/redispersion cycles, and then followed by pyridine treatment twice. Then the Mn concentrations measured from these nanocrystals were used to determine the concentration of the strongly bound Mn formed during dopant growth. After removing the weakly bound Mn, ICP measurements show that the concentrations of strongly bound Mn increase with dopant-growth time (Figure 3C). The formation of strongly bound Mn follows first-order kinetics, and the rate constants (k_2, Scheme 2) at the four different temperatures were extracted from linear

(58) Liu, H.; Owen, J. S.; Alivisatos, A. P. *J. Am. Chem. Soc.* **2007**, *129*, 305–312.

Scheme 2[a]
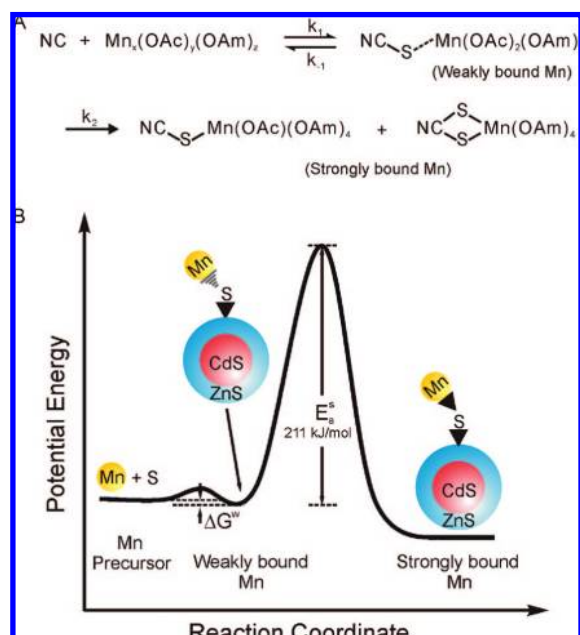
[a] (A) Proposed mechanism for the formation of the weakly and strongly bound Mn; NC (nanocrystal). Manganese acetate (the dopant precursor) may exist as a coordination polymer in reaction solutions.[58] (B) Proposed reaction profile for the formation of the weakly and strongly bound Mn. ΔG^w is the formation energy of weakly bound Mn, and E_a^s is the activation energy for the formation of strongly bound Mn.

Figure 4. Mn-GY after the dopant-growth and ZnS-shell-growth steps. The Mn concentration is 0.3 mM and the concentration of host particles is 6.3 μM. The host particles are 4.1-nm CdS/ZnS nanocrystals with core diameter of 3.1 nm and shell thickness of 0.5 nm, (A): with $Mn(OAc)_2$ + S (at molar ratio of 1:1) as dopant precursor; (B): with $Mn(OAc)_2$ + S (at molar ratio of 1:13) as dopant precursor; (C): with $Mn(S_2CNEt_2)_2$ as dopant precursor; Column *a:* taken after dopant growth for 20 min; Column *b:* taken after the growth of a 0.5-nm ZnS shell with the addition of zinc precursor first; Column *c:* taken after the growth of a 0.5-nm ZnS shell with the addition of sulfur precursor first.

curve fitting (Figure 3C).[56,57] In addition, the temperature dependence of these rate constants exhibits an Arrhenius behavior (Figure 3D).[56,57]

On the basis of the Arrhenius plot,[56,57] we obtained the activation energy ($E_a^s = 211 \pm 13$ kJ/mol) for the formation of strongly bound Mn (Figure 3D). This large activation-energy barrier indicates that the transition state of the formation of strongly bound Mn should be associated with the cleavage or formation of chemical bonds (Scheme 2). Furthermore, based on the Eyring equation,[56,57] we also extracted the entropy of activation ($\Delta S^{\ddagger} = 76.1$ J·mol^{-1}·K^{-1}) of the transition state from the Arrhenius plot (Figure 3D). The positive entropy of activation suggests that the rate-determining step in the formation of strongly bound Mn is a unimolecular decomposition reaction.[56,57] The cleavage of the Mn–O bond via the detachment of an acetate group in the weakly bound Mn complexes acts as the rate-determining step, because the Mn–O bond is the strongest bond in the complexes.[59] Then the rate-determining step is accompanied by the formation of the strong Mn–S bond, resulting in the strongly bound Mn on the surface of nanocrystals (Scheme 2).

To further confirm the reaction mechanism, we examined the possibility of converting the weakly bound Mn into strongly bound at a low temperature (220 °C). In principle, the cleavage of the Mn–O bond can be facilitated by a nucleophilic attack on the Mn atom by Lewis-base species (such as sulfur atoms). If the formation of strongly bound Mn is determined by the cleavage of the Mn–O bond, the presence of excess sulfur could facilitate the conversion of weakly bound Mn into strongly bound Mn.

To test this hypothesis, we used 4.1-nm CdS/ZnS nanocrystals as host particles to conduct a Mn-growth reaction at 220 °C
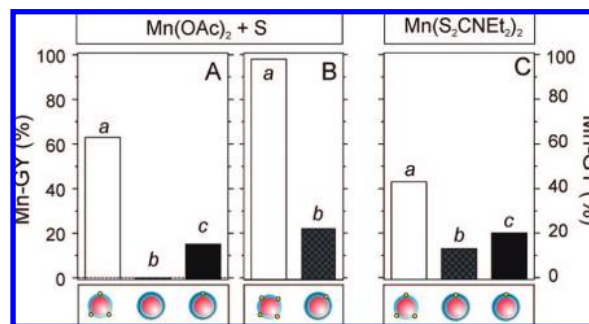
with Mn-acetate and sulfur as dopant precursors. The resulting particles were purified by three precipitation/redispersion cycles, and separated into two parts. One part of the sample was used in the control experiment in which the ZnS shell was grown starting with the addition of Zn-precursor. After ZnS-shell growth, a net Mn-growth yield of zero was found by ICP measurements, indicating no strongly bound Mn species were formed on the surface of CdS/ZnS nanocrystals in dopant growth (Figure 4A-b). Then the second part of the sample was used in an experiment in which the ZnS shell was grown starting with the addition of sulfur. In this experiment, CdS/ZnS nanocrystals with only weakly bound Mn had a chance to react first with sulfur alone for 10 min (the amount of sulfur is added for the growth of one monolayer of ZnS on 4.1-nm particles, S:Mn = 21:1), and then react with zinc stearate. After the ZnS-shell growth in this condition, the net Mn-growth yield is 15%, according to ICP measurements (Figure 4A-c). The results from these two experiments show that the reaction with sulfur can indeed lead to the conversion of weakly bound Mn into strongly bound on the surface of nanocrystals (Figure 4A-b,c). In addition, these results are consistent with the reaction mechanism that the cleavage of the Mn–O bond is the rate-determining step in the formation of strongly bound Mn.

Together, the results from all these studies strongly support the mechanism that Mn adsorption on the surface of nanocrystals includes two successive processes: the formation of weakly bound Mn and the formation of strongly bound Mn. Importantly, such a two-step, dopant-adsorption mechanism might also apply to the aqueous-phase doping synthesis. Indeed, Bryan et al. have proposed a similar mechanism for the adsorption of Co^{2+} onto the surface of CdS nanocrystals.[22] However, Bryan et al. suggested that the Co^{2+} adsorption is favored at a thermodynamic equilibrium in the aqueous reaction mixture.[22] In other words, the Co^{2+} adsorption is driven by a thermodynamic process, which is different from the kinetic-driven dopant adsorption in this work. This difference is due, in part, to the difference in synthesis solvents. Because water exhibits a strong solvation power, it makes sense that the Co^{2+} adsorption is determined by a thermodynamic equilibrium in aqueous-phase synthesis.[22] In contrast, the Mn adsorption in this work was conducted in organic solvents, which have a weak solvation capability for the dopant precursors. Therefore, reaction kinetics play the major role in the Mn adsorption described herein.

(59) Lide, D. R. *Handbook of Chemistry and Physics*, 84th ed.; CRC Press: Boca Raton, FL, 2003.

Effect of Dopant Precursor. To further confirm that the activation-controlled reaction kinetics are a determining factor in the formation of strongly bound Mn, we carried out experiments with constant temperature while varying the composition of Mn precursors. In general, the activation energy of a chemical reaction is determined by the reactivity of reactants: the higher the reactivity of reactants, the lower the activation energy needed to start the reaction.[57] Therefore, the use of active doping precursors could lead to the formation of strongly bound Mn at low-temperature growth condition such as 220 °C.

To examine this hypothesis, we chose an active doping precursor: manganese dithiocarbamate ($Mn(S_2CNEt_2)_2$), and conducted dopant growth and subsequent ZnS-shell growth at 220 °C. Indeed, the active doping precursor resulted in the formation of strongly bound Mn in the dopant-growth step, which is indicated by a net Mn-growth yield of 13% after ZnS-shell growth (Figure 4C-b). In contrast, a net Mn-growth yield of zero was obtained under similar conditions when Mn-acetate and sulfur were used as doping precursors (Figure 4 A-b). Moreover, the active doping precursor can also lead to the formation of weakly and strongly bound Mn; and an additional reaction with sulfur can also convert a part of weakly bound Mn into strongly bound ones (Figure 4C).

In addition, we found that dopant growth with Mn-acetate and sulfur as precursors at a large molar ratio (1:13, and with 48 Mn atoms per nanocrystal) can also lead to the formation of strongly bound Mn at 220 °C (Figure 4B). This dopant-growth condition results in CdS/ZnS core/shell nanocrystals with 48 Mn atoms bound on the surface (Figure 4B-a). About 22% of these Mn atoms are strongly bound Mn, which was determined by measuring the Mn-doping level of the resulting particles after subsequent ZnS-shell growth (Figure 4B-b). However, both TEM and high-resolution TEM measurements show that the resulting particles after this doping growth do not exhibit any measurable change in shape and surface morphology, as compared with those particles without strongly bound Mn, which was prepared in the experiment with Mn-acetate and sulfur at molar ratio of 1:1 (Figure 5). These results suggest that the formation of strongly bound Mn is not determined by nanocrystal shape and surface morphology, but just by the kinetics of the surface chemical reactions for Mn adsorption. Taken together, these results further confirm that the activation-controlled reaction kinetics are a determining factor for the chemical adsorption of Mn dopants onto the surface of host particles.

Replacement of Mn Dopants. The results from the previous sections show that weakly bound Mn on the surface of host particles can be removed by ZnS-shell growth, and specifically the Mn dopants are replaced by the incorporation of Zn atoms onto ZnS lattice sites. Here, a fundamental question is whether strongly bound Mn can be removed by ZnS-shell growth. This question is important for understanding the detailed nanocrystal-doping mechanism. If the answer is no, the Mn-doping level of final particles is just determined by the reactions for Mn adsorption. If yes, the Mn-doping level of final particles should also be determined by the reaction kinetics of Mn replacement.

To answer this question, we conducted seven sets of experiments to examine Mn-replacement yield as a function of the temperature of ZnS-shell growth (Figure 6A−B). To guarantee consistency in all these experiments, the CdS/ZnS core/shell nanocrystals with surface-bound Mn were prepared from the same batch of dopant-growth synthesis that was conducted at
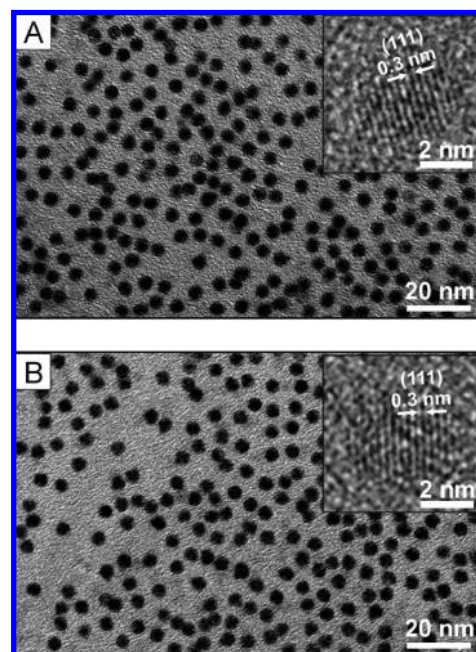

Figure 5. TEM images of CdS/ZnS core/shell nanocrystals with surface-bound Mn from the synthesis with $Mn(OAc)_2$ and sulfur as precursors with molar ratios of 1:1 (A) and 1:13 (B), respectively. (Insets) Typical high-resolution TEM images for the two nanocrystal samples.
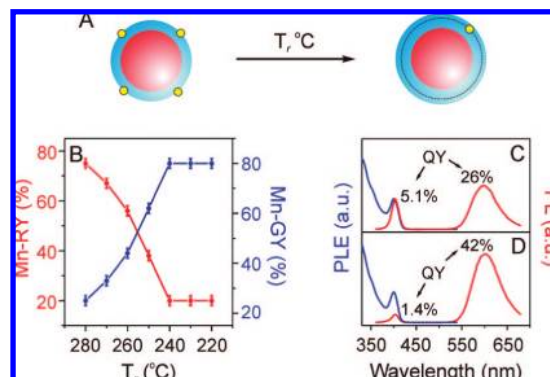

Figure 6. Study of Mn replacement. The concentration of host particles (4.1-nm CdS/ZnS nanocrystals) is 6.3 μM. (A): Scheme of experimental design. (B): Mn-replacement yield (Mn-RY, red) and Mn-growth yield (Mn-GY, blue) as a function of the temperature (T_r) for the growth of a 0.5-nm ZnS shell. (C): Photoluminescence excitation spectrum (blue) and photoluminescence spectrum (red) of the Mn-doped nanocrystals, which were synthesized with a dopant-growth temperature of 280 °C and a ZnS-shell-growth temperature of 280 °C. The Mn-precursor concentration is 0.09 mM (i.e., 15 Mn atoms per nanocrystal) and the ZnS-shell thickness is 4.8 monolayers. The final Mn-doping level is 0.11% (i.e., an average of 3.6 Mn atoms per nanocrystal), as measured by ICP. (D): Photoluminescence excitation spectrum (blue) and photoluminescence spectrum (red) of the Mn-doped nanocrystals, which were synthesized with a dopant-growth temperature of 280 °C and a ZnS-shell-growth temperature of 220 °C. The Mn-precursor concentration is 0.09 mM The final Mn-doping level is 0.35% (i.e., an average of 11 Mn atoms per nanocrystal), as measured by ICP.

280 °C with Mn-acetate and sulfur as precursor (1:13, 48 atoms per nanocrystal). The Mn-growth yield of nearly 100% was found in the doping-growth step and resulted in nanocrystals with an average of 48 Mn atoms on the surface. After ZnS-shell growth, the net Mn-growth yield was measured for each experiment. The Mn-replacement yield is determined as a ratio between the Mn-growth yields measured after and before ZnS-shell growth.

Experimental data show that ZnS-shell growth at 220, 230, and 240 °C resulted in a nearly identical Mn-replacement yield of about 20% (Figure 6B). These results suggest that weakly bound Mn on the surface of the nanocrystals is 20% before ZnS-shell growth. At higher temperatures, additional amounts of Mn are removed from the nanocrystal surface, and the Mn-replacement yield exhibits strong dependence on the temperature of ZnS-shell growth. The higher the growth temperature, the higher the replacement yield obtained and vice versa. These results further confirm our conclusion that two types of Mn species (i.e., weakly and strongly bound Mn) are formed in the dopant-growth step (Scheme 2). More importantly, these results demonstrate that ZnS-shell growth indeed removes some of the strongly bound Mn atoms from the surface of host particles at higher temperatures. The replacement reaction likely follows a cation-exchange reaction mechanism: Mn dopants are replaced from the surface of nanocrystals by the Zn atoms from zinc stearate. Therefore, the Mn-doping level of final particles is determined by the reaction kinetics of both the Mn adsorption and replacement processes.

In addition, the temperature-dependence of the replacement yields suggests that there is an activation-energy barrier required to start the Mn-replacement reaction. In the ZnS-shell-growth step, the Mn-replacement reaction and ZnS growth occur concurrently. ZnS growth can embed surface-bound Mn atoms into the ZnS lattice, and thus terminate the Mn-replacement reaction. Technically, it is very difficult to decouple these two reactions, and we did not quantitatively determine the activation-energy barrier for the Mn-replacement reaction in this work. However, it is still safe to conclude that the temperature-dependence of the Mn-replacement yield is due to overall effects from the reaction kinetics of Mn-replacement reaction and ZnS growth, in which both processes need to overcome their respective activation-energy barrier.

Based on this new understanding, one can easily control the kinetics of Mn replacement through the reaction temperatures, and thus can control the final Mn-growth yield for doped host particles (Figure 6B, blue curve, and Figure 6C–D). Indeed, the two Mn-doped CdS/ZnS nanocrystals made with ZnS-shell growth at different temperatures exhibit a clear difference in the intensity ratio of the band gap and Mn emission (Figure 6C–D). In addition, our results have demonstrated the ability to control the net Mn-growth yield between 25% and 80% by tuning the temperature of ZnS-shell growth (blue curve in Figure 6B). Note that the Mn-growth yield of 80% cannot be easily explained by the Norris model, which predicts a growth yield between zero and 30%.[6]

Fate of Replaced Mn Species. To produce high-quality nanocrystals with Mn dopants at controlled radial positions, we need to know the fate of those replaced Mn atoms in the reaction systems. Can those replaced Mn atoms be readsorbed onto the surface of host particles? If yes, it will be difficult to precisely control the Mn position inside host particles because of the incorporation of the replaced Mn during the subsequent ZnS-shell growth (Figure 7A-ii). To examine this possibility, we carried out six experiments that allow the mixture of Mn-doped particles and replaced Mn species to further react with sulfur at different excess amounts (Figure 7). In previous sections, we have obtained the result that the addition of sulfur can increase the concentration of adsorbed weakly bound Mn, and it can also convert weakly bound Mn atoms into strongly bound ones. In these six experiments, however, the reaction with additional sulfur did not affect the doping levels of the final products even
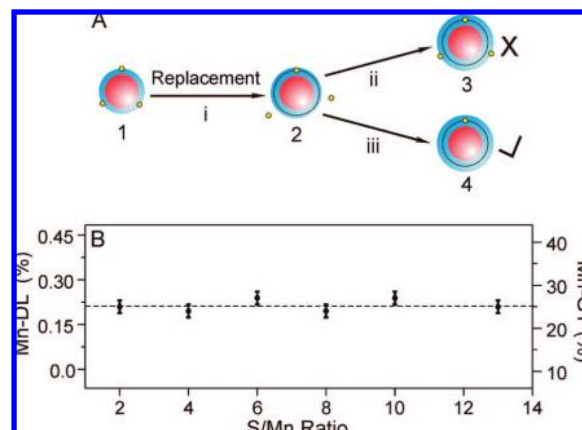

Figure 7. Mechanistic study to explore whether the replaced Mn species can be readsorbed onto doped nanocrystals. (A): Scheme of experimental design, (i) replacement reaction, (ii) and (iii): 0.5-nm ZnS shell is further grown onto the nanocrystals with surface-bound Mn.; (B): Mn-doping level (Mn-DL) and Mn-growth yield (Mn-GY) as a function of the amount of additional sulfur (S/Mn ratio). The Mn-precursor concentration is 0.3 mM, and the concentration of host particles is 6.3 μM.

up to 13 times excess sulfur (Figure 7B). This result demonstrates that the replaced Mn cannot be readsorbed onto the nanocrystal surfaces at these synthesis conditions. It indicates that the replaced Mn atoms form chemical species with very low reactivity, such as clusters with polymerized $(Mn-O)_n$ and $(Mn-S)_n$. Zinc stearate likely plays a major role in the formation of such Mn species in the cation-exchange reaction. Because the replaced Mn atoms cannot be reincorporated into the lattice of nanocrystals, one should be able to control the Mn radial position inside nanocrystals through such a three-step synthesis.[26]

Effects of Nanocrystal Size and Crystal Form. Nanocrystal size and crystal form have been found important to determining the Mn-growth yield in a one-pot doping synthesis, according to the reports from Norris et al.[6] However, a number of other researchers have suggested that nanocrystal size and crystal form have nearly no effects on dopant-growth yield.[60-62] Because it allows a more precise control of the size, crystal form, and concentration of host particles than the conventional one-pot doping synthesis used in these previous studies, our three-step synthesis was used to explore the effects of nanocrystal size and crystal form. To study the size effect, five sets of experiments were carried out for doping CdS/ZnS nanocrystals with sizes ranging from 3.6 to 5.6 nm. In the final products, Mn dopants are incorporated into the lattice of the ZnS-shell part of CdS/ZnS nanocrystals. ICP measurements show that Mn-growth yields are nearly identical among these experiments after both the dopant-growth and ZnS-shell-growth steps (Figure 8a–b). This preliminary result indicates that nanocrystal size is not a determining factor in the dopant incorporation for CdS/ZnS particles with sizes from 3.6 to 5.6 nm. This result does not contradict the results from Norris et al., because Mn-growth yield dramatically decreases only for very small particles (<2.0 nm).[6,60] However, our result herein provides more conclusive data on whether Mn-growth yield is size-dependent. This is because our result is obtained from experiments with well-

(60) Norberg, N. S.; Parks, G. L.; Salley, G. M.; Gamelin, D. R. *J. Am. Chem. Soc.* **2006**, *128*, 13195–13203.
(61) Nag, A; S.; Chakraborty, S.; Sarma, D. D. *J. Am. Chem. Soc.* **2008**, *130*, 10605–10611.
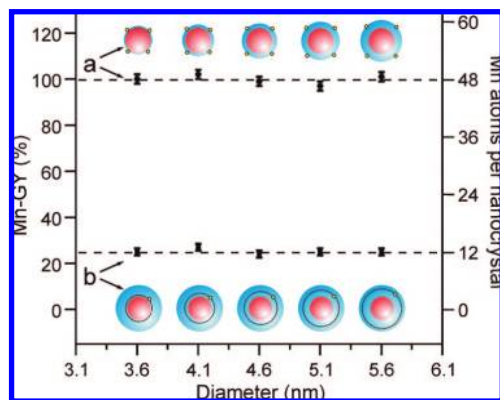(62) Jun, Y.; Jung, Y.; Cheon, *J. Am. Chem. Soc.* **2002**, *124*, 615–619.

Figure 8. Mn-growth yield (Mn-GY) and doping level (the number of Mn atoms per nanocrystal) as a function of the size of starting-host particles. Mn-GYs were measured after the steps of dopant growth (a) and ZnS-shell growth (b). The Mn-precursor concentration is 0.3 mM and the concentration of starting-host particles is 6.3 μM. The sizes of CdS/ZnS starting-host particles are 3.6, 4.1, 4.6, 5.1, and 5.6 nm, with CdS cores of the same size (3.1 nm). The final sizes of the Mn-doped CdS/ZnS nanocrystals are the same (6.2 nm).

Figure 9. Mn-growth yield (Mn-GY) as a function of the crystal form (zinc-blende and wurtzite) of CdS/ZnS core/shell nanocrystals. (A) Scheme of experimental design: Mn-GY was measured at the five stages during ZnS-shell growth: (B) for zinc-blende and (C) for wurtzite CdS/ZnS nanocrystals. XRD patterns of the Mn-doped CdS/ZnS nanocrystals taken from the final stage of ZnS-shell growth: (D) zinc-blende and (E) wurtzite. These Mn-doped CdS/ZnS nanoparticles have a diameter of 6.2 nm with a CdS core of 3.1 nm in diameter. The positions of standard XRD peaks for bulk zinc-blende and wurtzite ZnS are indexed in panels D and E, respectively.

controlled variables (i.e., the size and concentration of host particles), while the conventional one-pot synthesis used by Norris et al. cannot achieve such tight control over experimental variables.[6] Please note that Norberg et al. have shown that doping is size independent in a one-pot synthesis of Co^{2+}-doped ZnSe nanocrystals.[60]

To evaluate the effect of nanocrystal crystal form on dopant growth, we synthesized wurtzite CdS/ZnS nanocrystals according to the method reported by Steckel et al.[49] We then chose zinc-blende and wurtzite CdS/ZnS core/shell nanocrystals with nearly identical diameter (4.1 nm), CdS core diameter (3.1 nm) and ZnS-shell thickness (0.50 nm) as host particles for the dopant growth and ZnS-shell growth (Figure 9A). Dopant growth was conducted at 280 °C with Mn-acetate and sulfur as precursors (1:13, with 48 Mn atoms per nanocrystal). The Mn-growth yields are substantially different for the zinc-blende and wurtzite particles at the dopant-growth step, ~100% vs 60% (Figure 9B–C). This result seems consistent with the Norris model that claims that zinc-blende nanocrystals are superior to wurtzite ones for Mn-dopant growth.[6] After ZnS-shell growth at 280 °C, however, the Mn-growth yield was found to be similar (about 25%) in both syntheses at different shell thicknesses (Figure 9B–C). The resulting doped nanocrystals have a similar doping level, with an average of 12 Mn atoms per particle regardless of their crystal form. This result is inconsistent with the Norris model, as well as their experimental results on Mn-doping of CdSe nanocrystals.[6]

One possible reason for such a significant change in the Mn-growth yield between these two syntheses is that there is a crystal-structure change (from wurtzite to zinc blende) for wurtzite particles induced by ZnS-shell growth. Based on this possibility, our result here could still be explained by the Norris doping model. However, the possibility of crystal-form change is ruled out by the results from X-ray powder diffraction (XRD) measurements, which clearly show that the final products from these two syntheses have a zinc-blende and wurtzite crystal form (Figure 9D–E). Taken together, these results suggest that the crystal form of host particles is not a controlling factor in the formation of strongly bound Mn (or the final Mn-growth yield) in the doping synthesis. This conclusion is in agreement with our mechanism that nanocrystal doping is dependent on activa-
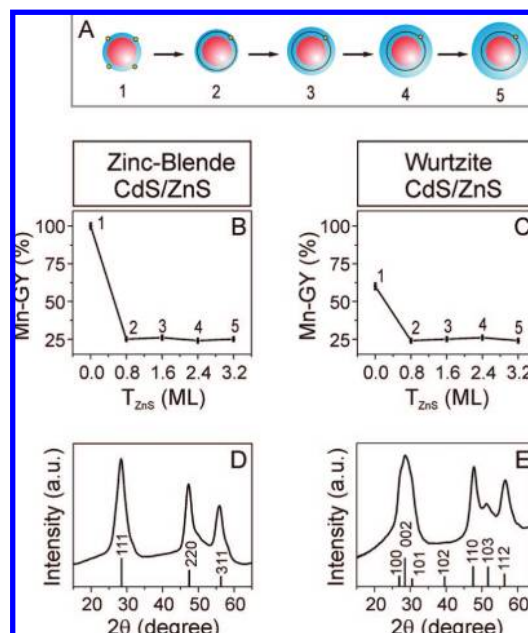
tion-controlled reaction kinetics. In addition, the significant difference in Mn-growth yield at the dopant-growth step is due to the difference in the yield of the weakly bound Mn formation. The lower formation yield for wurtzite particles could be caused, in part, by the strongly binding ligands on their surface (trioctylphosphine and bis(2,4,4-trimethylpentyl) phosphinic acid).[49] These ligands do not exist on the surface of zinc-blende particles.[26]

General Discussion. Based on the mechanistic study on the synthesis of Mn-doped CdS/ZnS nanocrystals, we can draw a few insights on nanocrystal doping in general. We first discuss the issue of surface-bound Mn. Surface-bound Mn has been a general issue in many studies on Mn-doped semiconductor nanocrystals.[20,35] The presence of surface-bound Mn can potentially lower the quality of doped nanocrystals.[20,35,46] Pyridine treatment is a widely used procedure to remove Mn ions from the surface of nanocrystals.[13,21,28] Gamelin et al. reported an efficient procedure for removing surface-bound Mn by heating ZnO nanocrystals in a solution of dodecylamine at 180 °C.[35] In our study, however, CdS/ZnS core/shell nanocrystals with surface-bound Mn are synthesized in OAm-rich solutions (ODE/OAm = 3:1), and the resulting surface-bound Mn includes both weakly bound and strongly bound Mn species. Our results show that alkylamine does not remove even weakly bound Mn from the surface of nanocrystals. In addition, our results are consistent with those from Norris et al., which show that a substantial amount of surface-bound Mn can exist on the ZnSe nanocrystals synthesized in hexadecylamine solutions at 260–300 °C.[20,21]

The inconsistency between our results and those reported by Gamelin et al., on the one hand, can be attributed to the difference in material compositions. On the other hand, it is

likely that zinc-acetate residuals in their samples play a major role in the replacement of surface-bound Mn from ZnO nanocrystals in Gamelin's experiments.[35] The second case is consistent with our observation that the Mn-doped CdS/ZnS nanocrystals obtained after ZnS-shell growth exhibit a very "clean" surface (Figure 1). In our studies herein, ZnS-shell growth is conducted in a solution of ODE and OAm (3:1) with zinc stearate and sulfur as precursors. The zinc acetate should play a similar role as zinc stearate in the replacement of surface-bound Mn. Indeed, our results have shown that the replaced Mn species should exist in low-reactivity forms and cannot be readsorbed on the surface of nanocrystals (Figure 7).

Second, we discuss the Mn adsorption and replacement on the surface of nanocrystals. Our kinetic studies have shown that the process of Mn adsorption starts from the formation of weakly bound Mn, and then is followed by a chemical reaction to form strongly bound Mn. The activation-energy barrier of the chemical reaction is 211 ± 13 KJ/mol when manganese acetate is used as doping precursor. This value is much higher than the typical barrier ($8-25$ kJ/mol) for a diffusion-controlled reaction,[57] and thus the formation of strongly bound Mn is not limited by diffusion, but by activation energy. In this study, we have shown two ways to control the kinetics: (1) the choice of reaction temperature: a higher temperature leads to a larger rate constant for the formation of strongly bound Mn (Figure 3); and (2) the choice of chemical composition of doping precursors (Figure 4): the higher reactivity of the precursors leads to a lower activation energy, and thus a faster reaction rate for the formation of strongly bound Mn on the surface of nanocrystals.

Moreover, our results have shown that both weakly bound and strongly bound Mn can be removed from the surface of nanocrystals by a cation-exchange reaction during ZnS-shell growth (Figures 2, 4, and 6). The replacement of strongly bound Mn occurs at temperatures higher than 250 °C, and overall Mn-replacement yield is strongly dependent on the ZnS growth temperature. The temperature-dependent behavior of the replacement yield is attributed to the overall effects from the reaction kinetics of Mn-replacement reaction and ZnS growth (Figure 6). Therefore, an increasing growth temperature will lead to an increase of reaction rates for both reactions, but fast ZnS growth can terminate the replacement reaction by embedding Mn atoms inside the ZnS lattice. Based on this understanding, one can control the Mn-replacement yield by tuning the temperature of ZnS-shell growth (Figure 6). In addition, one can lower the activation-energy barrier for ZnS-shell growth by using active growth precursors. Because it is determined by the intrinsic mechanism of the cation-exchange reaction, the activation energy of the Mn-replacement reaction might not be easily controlled. However, one can certainly use a low reaction temperature to minimize this replacement reaction. Moreover, the dopant-replacement reaction likely plays a major role in unsuccessful doping experiments using high growth temperatures (e.g., higher than 240 °C).[13,62] Furthermore, lattice strain might play a role in controlling the kinetics of dopant-replacement reaction. Indeed, Nag et al. have reported a very successful high-temperature synthesis of Mn-doped CdZnS alloy nanocrystals by fine-tuning the lattice parameters of host particles.[61]

Third, we discuss the general principles for the design of doping synthesis. Our results herein are consistent with a mechanism that nanocrystal doping is determined by the reaction kinetics of three processes: Mn-adsorption, replacement, and host-lattice growth. Specifically, our results suggest these three processes are under activation control. Accordingly, increases in reaction temperature lead to an increased reaction rate for all three processes, but the increased replacement rate will decrease the yield for Mn incorporation. Therefore, to achieve a successful nanocrystal doping synthesis, one can optimize the kinetics of three activation-controlled reactions by the choice of synthesis variables (e.g., reaction temperature, and chemical composition of precursors, which can tune the activation-energy barrier). For a conventional one-pot synthesis, only one reaction temperature can be used in a doping synthesis. Therefore, according to our doping mechanism, three criteria should be set for the design of such a synthesis: (1) a low reaction temperature, (2) high-reactivity dopant precursors, and (3) high-reactivity host-growth precursors (These precursors should allow dopant growth and host-lattice growth at this reaction temperature). Indeed, these three criteria are consistent with the synthesis conditions for many successful nanocrystal doping experiments in previous studies.[14,24,31,32] In contrast, a three-step synthesis allows the choice of different reaction temperatures for the dopant-growth and host-shell-growth steps. The design of such a synthesis is much more flexible in the choice of the chemical compositions of dopant precursors. For low-reactivity precursors, one can use a higher dopant growth temperature, and vice versa. For host-shell growth, one should use high-reactivity precursors, and thus a low growth temperature, which can decrease the reaction rate for the Mn-replacement reaction and maximize the reaction yield for the incorporation of Mn atoms into the lattice of nanocrystals (Figure 6).

Furthermore, if nanocrystal doping is determined by activation-controlled processes indicated by our results, it will be easy to understand the results for Mn-doping of wurtzite ZnO nanocrystals[35] as well as the doping synthesis using the active polychalcogenide precursors.[12,13,31] However, if the processes of dopant adsorption and host-lattice growth are under diffusion control, the kinetics of the dopant-replacement reaction will govern dopant incorporation. Then in the case that the rate-limiting step in the dopant-replacement reaction is a unimolecular dissociation of dopants from the nanocrystal surface, the dopant-replacement reaction will be determined by the dopant surface-binding energy. Then nanocrystal doping will follow the prediction of the Norris doping model, in which the shape and crystal structure of nanocrystals as well as ligand-binding energy are the determining factors.[6]

Conclusions

We report a mechanistic study on the Mn-doping of CdS/ZnS core/shell nanocrystals based on a three-step synthesis. This work provides a number of important conclusions. First, Mn adsorption on the surface of nanocrystals includes two successive processes: the formation of weakly bound Mn, and the formation of strongly bound Mn. The formation of weakly bound Mn is associated with a chemical equilibrium between adsorbed Mn species on the nanocrystal surface and the free Mn species in the reaction solution. The formation of strongly bound Mn is determined by a unimolecular decomposition reaction with an activation-energy barrier of 211 ± 13 kJ/mol. Second, both weakly bound and strongly bound Mn can be removed during ZnS-shell growth. The replacement of weakly bound Mn can occur at or below 240 °C, while the replacement of strongly bound Mn requires a higher temperature. The reaction yield of replacement is strongly dependent on ZnS-growth temperature, suggesting that the Mn replacement needs

to overcome an activation-energy barrier. Third, with well-controlled experimental variables (i.e., the size, shape, and concentration of host particles), we found that the overall Mn-growth yield is not dependent on the size, shape and crystal form of CdS/ZnS core/shell nanocrystals. Taking all these results together, we propose a nanocrystal doping mechanism in which dopant incorporation is determined by three activation-controlled processes: dopant adsorption, dopant replacement, and host-lattice growth. Based on this doping mechanism, one can easily control dopant incorporation through optimizing these three processes by the choice of reaction temperatures and the chemical compositions of dopant- and host-growth precursors. In this way, the recent advances in controlling colloidal nanocrystal synthesis may become extremely useful in optimizing the dopant-growth yield for nanocrystal doping synthesis.

Furthermore, our results could be generalized for doping nanocrystals of other compositions and with other impurities (e.g., indium and cobalt, but these impurities should have a negligible diffusion coefficient inside the host lattice at typical synthesis temperatures (<300 °C)).[59]